Beta dependence of electron heating in decaying whistler turbulence: Particle-In-Cell simulations

S. Saito[1, a)] and S. Peter Gary[2, b)]

[1)] *National Institute of Information and Communications Technology 4-2-1, Nukui-Kitamachi, Koganei, Tokyo, 184-8795, Japan*

[2)] *Los Alamos National Laboratory, Los Alamos New Mexico 87545, USA*

(Dated: 22 September 2011)

Two-dimensional particle-in-cell simulations have been carried out to study electron beta dependence of decaying whistler turbulence and electron heating. Initially applied whistler fluctuations in relatively long wavelengths cascades their fluctuation energy into shorter wavelengths. The development leads to whistler turbulence with anisotropic wavenumber spectra which are broader in directions perpendicular to the magnetic field than in the parallel direction. Comparing development of whistler turbulence at different electron beta values, it is found that the anisotropy of the wavenumber spectrum and relative electron heating decreases with increasing beta. The effective dissipation of obliquely propagating whistlers reduces the perpendicular energy cascade of whistler turbulence. As a result, energy dissipation by electron Landau damping responsible for the electron parallel heating becomes weaker at higher beta values. Therefore, at high beta, like conditions in the solar wind at 1AU, electron kinetic processes are important in determining the properties of whistler turbulence. This kinetic property is applied to discuss the generation of suprathermal strahl electron distributions in the solar wind.

PACS numbers: Valid PACS appear here

Keywords: whistler wave, short-scale turbulence, solar wind, wave-particle interaction

[a)]Electronic mail: ssaito@nict.go.jp

[b)]Electronic mail: pgary@lanl.gov

I. INTRODUCTION

Solar wind magnetic turbulence is observed to have power law energy spectra in frequency observed in a spacecraft frame of reference f'. In the magnetohydrodynamics (MHD) regime where f' is less than 0.1Hz, the spectral index is frequently close to $-5/3$[1,2]. Because of the power-law similarity with isotropic neutral fluid turbulence which also has the index $-5/3$, the MHD range in the solar wind turbulence is termed the inertial range. The spatial scales of the inertial range are longer than the proton inertial length λ_p or the proton Larmor length ρ_p which correspond to $f' < 0.1$Hz, assuming the Taylor frozen-in-flow hypothesis.

The energy cascade of solar wind turbulence transfers its energy in the inertial range into a short scale turbulence range which is usually observed at $f' > 0.1$Hz. The magnetic spectrum at the short scales has a spectral breakpoint, and is usually steeper than the inertial range[1,3,4]. Some earlier papers describe the steep energy spectra as "dissipation range" again because of a similarity with fluid turbulence. The MHD cascade supplies its fluctuation energy into the dissipation range, and the energy is transferred into plasma thermal energy there.

Indeed, without dissipation of the MHD turbulence, it is difficult to explain the radial trends of solar wind temperatures. Marsch *et al.*[5] showed that the proton temperature has a flatter power-law dependence over radial distance R between 0.3 and 1 AU than the dependence R^{-2} which one would expect if the first adiabatic invariant of the protons were conserved. Further they found the proton temperature anisotropy $T_{\perp,p} > T_{\parallel,p}$, where $T_{\perp,p}$ and $T_{\parallel,p}$ are proton temperature perpendicular and parallel to the background magnetic field, respectively. The observational results strongly suggest that perpendicular proton heating occurs in the solar wind. This could be a signature of pitch angle scattering through wave-particle interactions between parallel-propagating Alfvénic fluctuations and protons. However, as concluded by Leamon *et al.*[3], parallel-propagating Alfvén cyclotron fluctuations are inconsistent with the observational data at short scales. This suggests that the short scale regime consist of other weakly damped fluctuations, such as kinetic Alfvén[3] and whistler fluctuations[6]. Gary and Smith[6] have used linear theory to conclude that both whistler and kinetic Alfvén modes between proton inertial and electron inertial scale probably contribute to the short scale turbulence in the solar wind. Both fluctuations are dispersive at such scales, so this regime has also been called the "dispersion range".

Recent solar wind observations show that the dispersion range of magnetic spectra extends into the electron scales. Sahraoui *et al.*[7,8] found a second spectral break at $\sim \lambda_e$ or $\sim \rho_e$ with still steeper magnetic spectrum beyond those scales. They argue that kinetic Alfvén turbulence is responsible for the dispersion range in the solar wind at 1AU, and electron Landau damping dissipates the fluctuation energy at scales beyond the second spectral breakpoint. Gyrokinetic simulations for kinetic Alfvén turbulence at scales longer than the dissipation scales show a steep magnetic spectrum with spectral index ~ -2.6 which corresponds to the observations of solar wind turbulence at 1AU[4,7]. Leamon *et al.*[3] have also suggested that the kinetic Alfvén fluctuations are in the dispersion range; however, Podesta *et al.*[9] argue that such fluctuations cannot reach electron scales in the solar wind at 1AU because of their dissipation. This suggests that whistler fluctuations that have relatively weak damping close to the electron scales can be responsible for the very steep magnetic spectrum beyond the second spectral break. So whistlers may have an important role to heat electrons at the end of the dispersion range.

Some studies of homogeneous whistler turbulence have used the electron magnetohydrodynamics (EMHD) model. This model describes plasma behavior at wavelengths shorter than the ion inertial length λ_i, and assumes the ions are at rest and the electrons are represented as a single fluid. Under the EMHD model, computer simulations show a forward cascade of an initial ensemble of relatively long-wavelength whistlers to larger wavenumbers, yielding omnidirectional magnetic energy spectra which scale as $\propto k^{-7/3}$ in both two-dimensional[10,11] and three-dimensional simulations[12,13] over $|k\lambda_e| < 1$. Furthermore, both analytic theories[14] and computations[13] show that whistler turbulence in the magnetized EMHD model is anisotropic in wavenumber space, evolving to a state in which there is more magnetic fluctuation energy at wavevectors relatively perpendicular to the background magnetic field than parallel.

The EMHD model does not represent the kinetic properties of the electrons, and therefore cannot describe the consequences of collisionless processes such as Landau or cyclotron damping. Generally kinetic processes are sensitive to changes in the plasma environment such as the ratio of plasma thermal and magnetic field energies, defined as the plasma beta. At higher beta whistler waves are more easily dissipated at electron scales. Therefore, the EMHD model is not suitable to demonstrate electron heating by whistler turbulence in the solar wind which has a variable beta. In contrast particle-in-cell (PIC) simulations com-

pute velocity-space dynamics of both electrons and ions, and thus provide insight into how such processes contribute to plasma evolution. Recent two-dimensional PIC simulations[15–19] considered the evolution of whistler turbulence in homogeneous, collisionless, magnetized plasmas. In each case a spectrum of relatively long wavelength whistlers ($|k\lambda_e| < 0.2$) is imposed as an initial condition, and the fluctuations are allowed to freely decay in time. Each exhibits the development of an anisotropic broad band turbulent spectrum via a forward cascade which consistently leads to short wavelength fluctuations propagating perpendicularly or quasi-perpendicularly to the background magnetic field. These PIC simulations[15,16] at electron beta $\beta_e = 0.1$ show the anisotropic wavenumber spectra and anisotropic electron heating through electron Landau resonance which preferentially increases thermal energy parallel to the background magnetic field. Saito *et al.*[18] have done a simulation at $\beta_e = 0.01$ where wave-particle dissipation is weak. They found a more anisotropic wavenumber spectrum than at $\beta_e = 0.1$. All of these runs show results qualitatively similar to those from the EMHD models.

Here two-dimensional particle-in-cell simulations of whistler turbulence are carried out in a collisionless, homogeneous, magnetized plasma at three plasma beta values, in order to study the role of whistler turbulence on electron heating in the solar wind that has a variable plasma beta. Our simulation results show that at higher plasma beta values the magnetic energy cascade in the perpendicular direction becomes weaker and leads to more isotropic wavenumber spectra. Dissipated fluctuation energy heats electrons and increases their kinetic energy. We have found that the electron energy gains parallel and perpendicular to the magnetic field become comparable at high beta.

II. SIMULATION MODEL AND PARAMETERS

We have done two-dimensional and three-velocity (2D3V) relativistic electromagnetic particle-in-cell simulations, using the TRISTAN code[20]. This simulation model solves the full kinetic properties of the plasma using Maxwell equations for electromagnetic fields and the equations of motion for both electrons and protons. Wave-particle interactions are fully calculated in this model, contrary to fluid simulations such as MHD and EMHD model.

We use 1024×1024 grid points in the two-dimensional simulation box on the x-y plane, where the periodic boundary condition for the two directions is imposed on particles and

fields. The z direction is defined as the direction perpendicular to the two-dimensional plane. A grid cell size Δ is same everywhere in the simulation box. The number of electron-proton pairs in the cell is 64, so the total number of pairs is about 6.7×10^7. We define the light speed, particle mass, thermal speed, plasma frequency, and cyclotron frequency as c, m_j, $v_{t,j}$, ω_j, and Ω_j. A subscript "j" indicates electron ($j = e$) or proton ($j = p$) species. The mass ratio of electron and proton is $m_p/m_e = 1836$. The Debye length $v_{t,j}/\omega_j$ of electrons and protons are comparable to the grid cell size, when the electron temperature is same as proton $T_p = T_e$. The electron and proton inertial lengths are $\lambda_e = c/\omega_e = 10\Delta$ and $\lambda_p = c/\omega_p = \sqrt{1836}\lambda_e$ respectively. The simulation time step is $\delta t = 0.05/\omega_e$. We use relatively large electron thermal speed $v_{t,e} = 0.1c$ to reduce calculation costs. To study plasma beta dependence of whistler turbulence, we use different values of the background magnetic field B_0 along x direction.

We impose 42 right-hand polarized whistler fluctuations at t=0 in the two-dimensional simulation box. Wavenumbers of the fluctuations are $k_x\lambda_e = \pm 0.0613m$, $k_y\lambda_e = 0$, and $k_y\lambda_e = \pm 0.0613m$ (m=1-3). Frequencies of the imposed fluctuations are derived from the linear dispersion relation in a homogeneous collisionless plasma. The fluctuating magnetic field $\delta\mathbf{B}_n$, electric field $\delta\mathbf{E}_n$, and electric current density $\delta\mathbf{J}_n$ of each mode satisfy Faraday's and Ampere's equations. Here the subscript n is the mode number. The electrostatic component of obliquely propagating whistler fluctuations at t=0 is neglected to make a more simple initial condition. The energy composition of electrostatic fluctuations is quite weak compared with the electromagnetic, so we expect that self-consist electrostatic component must be generated during a short time scale such as a few plasma periods. Under this condition, Saito *et al.*[16] have demonstrated that whistler fluctuations keep linear dispersion properties after whistler turbulence is well developed. The electric current density is carried only by electrons, assuming that protons are at rest due to their large inertia in this relatively high frequency regime. At t=0, each fluctuation has an equal fluctuating amplitude, while phases are chosen using a uniform random function. The initial magnetic field energy relative to the background magnetic field energy is defined as $\epsilon_B = \sum_{n=1}^{42} (|\mathbf{B}_n|^2/B_o^2)$.

III. PARTICLE-IN-CELL SIMULATION RESULTS

In this section, we show simulation results of decaying whistler turbulence with $\epsilon_B = 0.1$ in electron beta values $\beta_e = 0.01$, 0.1, and 1.0.

A. Beta dependence of decaying whistler turbulence

Figure 1 shows time histories of magnetic fluctuation energy

$$E_B = \sum \frac{|\delta \mathbf{B}(k_x, k_y)|^2}{B_0^2}, \tag{1}$$

summed over wavenumbers $0.3 \leq k \leq 3.0$ in $\beta_e = 0.01$ (green), 0.1 (blue), and 1.0 (red). Here wavenumber k is $\sqrt{k_x^2 + k_y^2}$. Since the wavenumber range excludes initially applied whistlers, Figure 1 indicates the time development of the forward cascaded magnetic fluctuation energy. The cascaded energy increases in early phase of all three simulations, but the dissipation at short wavelengths decreases the fluctuation energy at later times. As the plasma beta increases, much less fluctuation energy is available to maintain the cascading short wavelength fluctuations. The relatively high plasma beta provides strong dissipation and small energy cascade rate (because the magnetic fluctuation energy $|\mathbf{B}^2 = \epsilon_B B_0^2|$ is smaller at higher beta values), so the cascaded magnetic fluctuation energy is smaller than the corresponding energy in the lower beta values. The fluctuation energies are almost saturated at $|\Omega_e|t \sim 500$, 2000, and 3000 at $\beta_e = 1.0$, 0.1, and 0.01 respectively.

Figure 2 shows two-dimensional wavenumber spectra of magnetic fluctuation energy $|\delta \mathbf{B}(k_x, k_y)|^2/B_0^2$ for the same three simulations at the saturated times as seen in Figure 1. Here the color contours are in log-scale. The two-dimensional wavenumber spectra show anisotropic features that preferentially transfer their fluctuation energy into the k_y direction. The anisotropic feature becomes less clear at larger beta values. The k_x spectra at small k_y are similar in the three cases, but the k_y spectra at small k_x become narrow with increasing beta. This indicates that the anisotropy of wavenumber space decreases with increasing beta.

Figure 3 shows time histories of wavenumber spectral anisotropy for the three simulations, which is defined as[21]

$$\tan^2 \theta_B = \frac{\sum_k k_y^2 |\delta \mathbf{B}(k_x, k_y)|^2}{\sum_k k_x^2 |\delta \mathbf{B}(k_x, k_y)|^2}. \tag{2}$$

where θ_B is spectral anisotropy angle. The time histories of the anisotropy $\tan^2\theta_B$ for all three simulations are saturated at late times which almost correspond to the saturated times of cascaded magnetic fluctuation energy seen in Figure 1. The saturated value of the anisotropy decreases with increasing beta, indicating that the wavenumber spectra become more isotropic at larger beta values as seen in Figure 2. Electron cyclotron damping is predominantly a function of k_x, whereas electron Landau damping is a function of both k_x and k_y, so Figure 2 and 3 clearly demonstrate that the increasing beta corresponds to the increase of electron Landau damping. Fluctuation energies dissipated through the electron Landau and electron cyclotron damping heats electrons in both the parallel and perpendicular directions.

B. Beta dependence of electron heating

Figure 4 shows reduced electron velocity distributions $f_e(v_x,t)$ and $f_e(v_y,t)$ at $t=0$ (red solids) and late times (blue dashed) for the same three simulations. These are normalized to the maximum value of the distribution at $t=0$. Both parallel and perpendicular electron heating occur at late times. The electron Landau damping associated with the obliquely propagating whistlers scatters electrons in the parallel direction, so the parallel heating is more effective than perpendicular heating in the anisotropic whistler turbulence. The initial magnetic fluctuation energy $|\delta\mathbf{B}|^2 = \epsilon_B B_0^2$ relative to the electron kinetic energy density $m_e\kappa_B T_e$ becomes smaller at higher beta values, so the overall heating is weaker, as seen in the reduced velocity distributions.

Figure 5 shows the anisotropic heating ratio of electrons for the three simulations defined as

$$\eta_e = \frac{(K_{e,y} - K_{0,e,y}) + (K_{e,z} - K_{0,e,z})}{2(K_{e,x} - K_{0,e,x})} \tag{3}$$

where K_e is the electron kinetic energy summed over all electrons. Subscripts "0" indicates the kinetic energy at $t=0$. The denominator is close to be zero in early phase, so we plot this at $\Omega_e t > 200$. This panel clearly shows that the electron heating by whistler turbulence is more isotropic at higher beta values. The anisotropic heating ratio gradually increases in time. This would be due to the electron cyclotron resonance heating electrons in the perpendicular direction.

Figure 6 shows anisotropic heating ratio of electrons for three simulations with $\epsilon_B = 0.02$,

0.1, and 0.2 at $\beta_e = 0.1$, which we additionally have done to confirm the plasma beta is responsible for the anisotropies of wavenumber spectrum and electron heating, rather than $|\delta\mathbf{B}|^2$ $(= \epsilon_B B_0^2)$. The development of the anisotropic heating ratio with different fluctuation amplitudes are almost comparable. If the heating rates of the parallel and perpendicular temperature components are due to linear Landau damping and linear cyclotron damping, respectively, the η_e should be relatively independent of fluctuation amplitudes. So the results of Figure 6 are consistent with the hypothesis that electron heating in our simulations is due to these two linear dissipation processes rather than nonlinear dissipation processes.

IV. DISCUSSION AND CONCLUSION

We have done two-dimensional particle-in-cell simulations for whistler turbulence at low ($\beta_e = 0.01$), middle ($\beta_e = 0.1$), and high ($\beta_e = 1.0$) plasma beta condition. Our simulations show that the anisotropies of magnetic wavenumber spectrum of decaying whistler turbulence and electron heating decreases with increasing plasma beta.

The cascaded fluctuation energy should finally be dissipated and converted into the electron kinetic energy, so the cascade rate could be almost proportional to the heating rate. Our simulation results, showing that the electron heating of parallel and perpendicular directions becomes more isotropic at higher beta values, imply that a ratio of energy cascade rates between the parallel and perpendicular directions becomes more isotropic at higher plasma beta values.

In linear theory, the Landau damping associated with wavenumber perpendicular to the background magnetic field becomes effective at high beta. The effective damping for obliquely propagating whistlers prevents fluctuation energy cascade in wavenumber perpendicular to the background magnetic field. We expect that this leads to more isotropic energy cascade rate of whistler turbulence at higher beta values, and then electron heating becomes more isotropic. Our simulation results indicate that electron kinetic processes are important in determining the properties of whistler turbulence and electron heating.

In decaying whistler turbulence, the relative gain of electron kinetic energy becomes weak with increasing beta, because of lack of initial fluctuation energy compared with the electron thermal energy. In a realistic situation such as the solar wind where the fluctuation energy in the inertial range is continuously transferred into the dispersion/dissipation range, we expect

that electrons strongly dissipate the cascaded fluctuations. Electrons would be heated more isotropically at higher beta conditions by whistler turbulence.

We propose that the beta dependence of electron heating by whistler turbulence may be responsible for generation of the solar wind suprathermal electron strahl distribution, which is a relatively high energy component with narrow pitch angle distribution streaming in the anti-sunward direction. Vocks and Mann [22] proposed the following process for strahl generation by using quasilinear theory: (1) Electrons moving in the sunward direction parallel to the magnetic field are scattered by whistler waves propagating in the anti-sunward direction along the magnetic field. (2) This wave-particle interactions increase the electron kinetic energy and pitch angle. (3) The magnetic mirror force of the opening magnetic structure reflects the accelerated (scattered) electrons and focuses these electrons toward the narrow strahl distribution.

This scenario would be one plausible mechanism to generate the strahl distribution; however, they did not discuss the beta dependence of the strahl distribution as seen in the solar wind observations[23–25]. The strahl distribution almost vanishes in sector boundaries of the interplanetary magnetic field where plasma beta is relatively high, whereas the strahl electrons have extremely narrow distributions far from sector boundaries where the plasma beta is relatively low. In order to generate the strahl electrons, this fact requires other wave-particle interaction processes beyond the electron cyclotron resonance. In a regime of whistler turbulence, electron Landau resonance would be an important role to explain the beta dependence of the strahl generation. At relatively low beta, far from sector boundaries, whistler turbulence scatters electrons preferentially parallel to the magnetic field as shown in Figure 5. The accelerated electrons are further focused in velocity space because of the magnetic mirror force associated with the opening magnetic field structure, and then form the strahl distribution. At relatively high beta conditions, like at sector boundaries of the magnetic field, the electron scattering by whistler turbulence tends to be more nearly isotropic. Electrons are not preferentially accelerated along the magnetic field, so we expect that the strahl distribution does not appear in the sector boundaries of the interplanetary magnetic field. Properties of whistler turbulence including kinetic processes would be one plausible generation mechanism of suprathermal electron strahl distributions in the solar wind.

ACKNOWLEDGMENTS

This work was supported by Grant-in-Aid for Young Scientists (B) Grant No. 21740353 from Japan Society for the Promotion of Science. The Los Alamos portion of this work was performed under the auspices of the U.S. Department of Energy (DOE). It was supported by the Solar and Heliospheric Physics SR&T and Heliophysics Guest Investigators Programs of the National Aeronautics and Space Administration.

REFERENCES

[1]C. W. Smith, B. J. Vasquez, and K. Hamilton, J. Geophys. Res. **111**, A09111 (2006).

[2]J. J. Podesta, D. A. Roberts, and M. L. Goldstein, Astrophys. J. **664**, 543 (2007).

[3]R. J. Leamon, C. W. Smith, N. F. Ness, and W. H. Matthaeus, J. Geophys. Res. **103**, 4775 (1998).

[4]C. W. Smith, K. Hamilton, B. J. Vasquez, and R. J. Leamon, Astrophys. J. Lett. **645**, L85 (2006).

[5]E. Marsch, K.-H. Muhlhauser, R. Schwenn, H. Rosenbauer, W. Pilipp, and F. M. Neubauer, J. Geophys. Res. **87**, 52 (1982).

[6]S. P. Gary and C. W. Smith, J. Geophys. Res. **114**, A12105 (2009).

[7]F. Sahraoui, M. L. Goldstein, P. Robert, and Y. V. Khotyaintsev, Phys. Rev. Lett. **102**, 211102 (2009).

[8]F. Sahraoui, M. L. Goldstein, G. Belmont, P. Canu, and L. Rezeau, Phys. Rev. Lett. **105**, 131101 (2010).

[9]J. J. Podesta, J. E. Borovsky, and S. P. Gary, Astrophys. J. **712**, 685 (2010).

[10]D. Biskamp, E. Schwarz, and J. F. Drake, Phys. Rev. Lett. **76**, 1264 (1996).

[11]D. Shaikh and G. P. Zank, Phys. Plasmas **12**, 122310 (2005).

[12]D. Biskamp, E. Schwarz, A. Zeiler, A. Celani, and J. F. Drake, Phys. Plasmas **6**, 751 (1999).

[13]J. Cho and A. Lazarian, Astrophys. J. Lett. **615**, L41 (2004).

[14]S. Galtier and A. Bhattacharjee, Phys. Plasmas **10**, 3065 (2003).

[15]S. P. Gary, S. Saito, and H. Li, Geophys. Res. Lett. **35**, L02104 (2008).

[16]S. Saito, S. P. Gary, H. Li, and Y. Narita, Phys. Plasmas **15**, 102305 (2008).

[17]S. P. Gary, S. Saito, and Y. Narita, Astrophys. J. **716**, 1332 (2010).
[18]S. Saito, S. P. Gary, and Y. Narita, Phys. Plasmas **17**, 122316 (2010).
[19]E. Camporeale and D. Burgess, Astrophys. J. **730**, 114 (2011).
[20]O. Buneman, "Computer space plasma physics: Simulation techniques and software," (Terra Sci., 1993) Chap. 3, p. 67.
[21]J. V. Shebalin, W. H. Matthaeus, and D. Montgomery, J. Plasma Physics **29**, 525 (1983).
[22]C. Vocks and G. Mann, Astrophys. J. **593**, 1134 (2003).
[23]W. G. Pilipp, H. Miggenrieder, K.-H. Muhlhauser, H. Rosenbauer, R. Schwenn, and F. M. Neubauer, J. Geophys. Res. **92**, 1103 (1987).
[24]W. G. Pilipp, H. Miggenrieder, M. D. Montgomery, K.-H. Muhlhauser, H. Rosenbauer, and R. Schwenn, J. Geophys. Res. **92**, 1075 (1987).
[25]N. U. Crooker, D. E. Larson, S. W. Kahler, S. M. Lamassa, and H. E. Spence, Geophys. Res. Lett. **30**, 1619 (2003).

FIGURE CAPTIONS

Figure 1

Time histories of magnetic fluctuation energy summed over wavenumbers $0.3 \leq k \leq 3.0$, where wavenumber k is $\sqrt{k_x^2 + k_y^2}$. Green, blue, and red line indicate $\beta_e = 0.01$, 0.1, and 1.0, respectively.

Figure 2

Two-dimensional wavenumber spectra of magnetic fluctuation energy $|\delta\mathbf{B}(k_x, k_y)|^2/B_0^2$ for the three simulations at saturated times which are defined as $|\Omega_e|t = 500$ at $\beta_e = 1.0$, $|\Omega_e|t = 2000$ at $\beta_e = 0.1$, and $|\Omega_e|t = 3000$ at $\beta_e = 0.01$, as seen in Figure 1.

Figure 3

Time histories of wavenumber spectral anisotropy of magnetic fluctuations at $\beta_e = 0.01$ (green), 0.1 (blue), and 1.0 (red).

Figure 4

Reduced electron velocity distributions at $t = 0$ (solid red lines) and saturated times (dashed blue lines). The saturated times are defined as $|\Omega_e|t = 500$ at $\beta_e = 1.0$, $|\Omega_e|t = 2000$ at $\beta_e = 0.1$, and $|\Omega_e|t = 3000$ at $\beta_e = 0.01$, as seen in Figure 1. These distributions are normalized to the maximum value at $t = 0$.

Figure 5

Time histories of anisotropic heating ratio of electrons for the three simulations defined as η_e at $\beta_e = 0.01$ (green), 0.1 (blue), and 1.0 (red).

Figure 6

Time histories of η_e for three simulations with $\epsilon_B = 0.02$ (green), 0.1 (blue), and 0.2 (red) at $\beta_e = 0.1$.

Figure 1

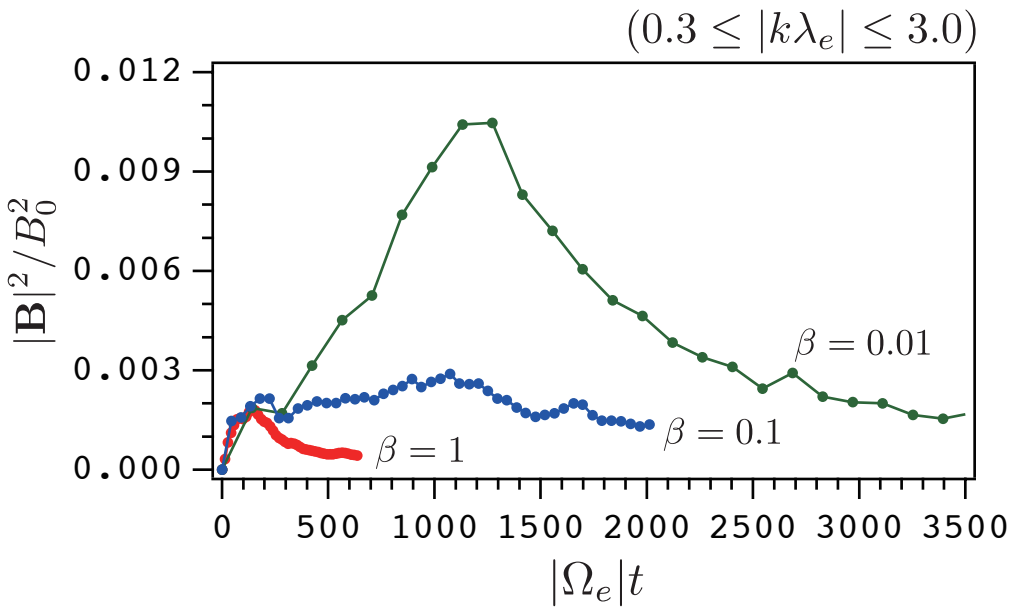
$(0.3 \leq |k\lambda_e| \leq 3.0)$
0.012
0.009
0.006
0.003
0.000
$|\mathbf{B}|^2/B_0^2$
$\beta = 0.01$
$\beta = 0.1$
$\beta = 1$
0
500
1000
1500
2000
2500
3000
3500
$|\Omega_e|t$

Figure 2

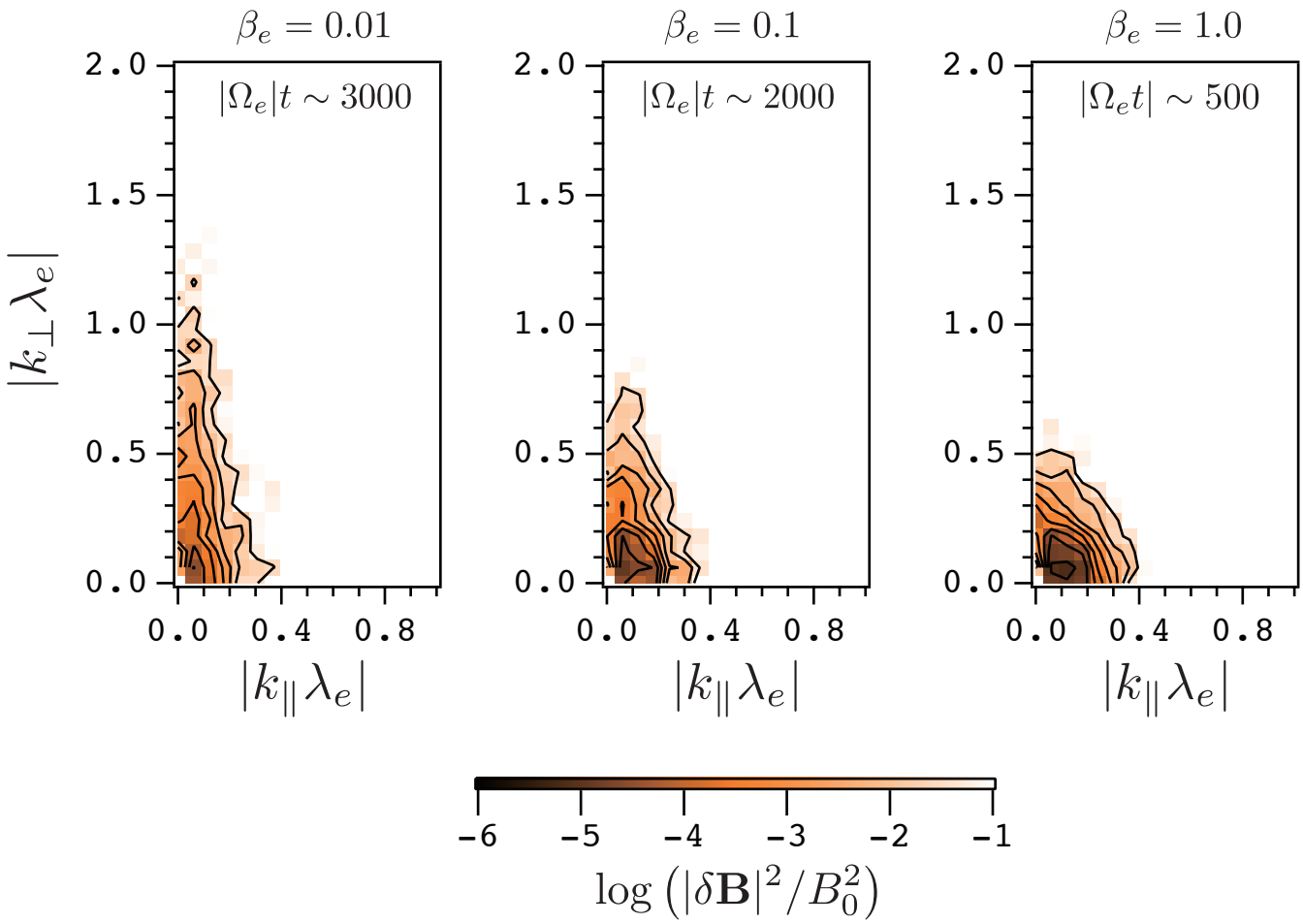
$\beta_e = 0.01$
$\beta_e = 0.1$
$\beta_e = 1.0$
$|\Omega_e|t \sim 3000$
$|\Omega_e|t \sim 2000$
$|\Omega_e t| \sim 500$
$|k_\perp \lambda_e|$
$|k_\parallel \lambda_e|$
0.0
0.5
1.0
1.5
2.0
0.4
0.8
−6
−5
−4
−3
−2
−1
$\log\left(|\delta\mathbf{B}|^2/B_0^2\right)$

Figure 3

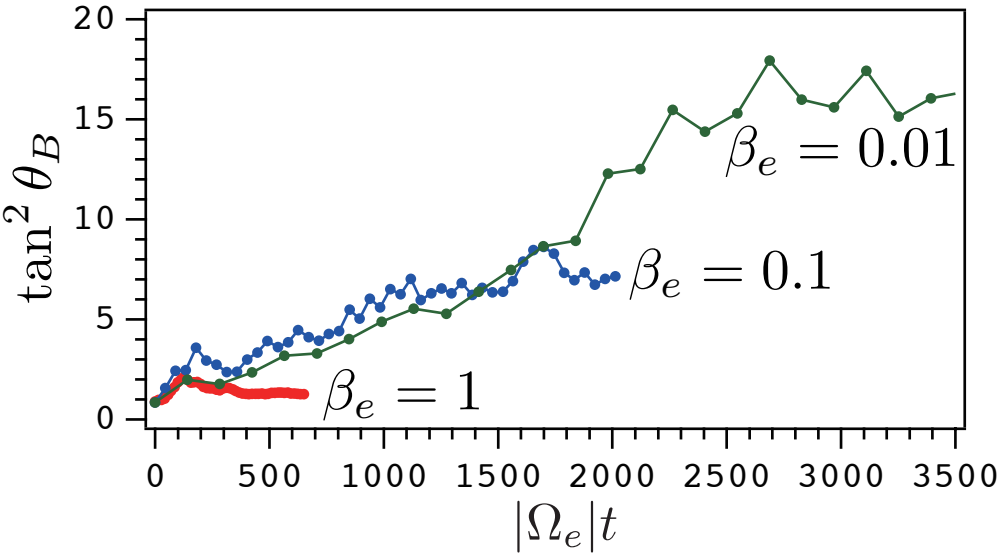
20
15
10
5
0
$\tan^2\theta_B$
0
500
1000
1500
2000
2500
3000
3500
$|\Omega_e|t$
$\beta_e = 0.01$
$\beta_e = 0.1$
$\beta_e = 1$

Figure 4

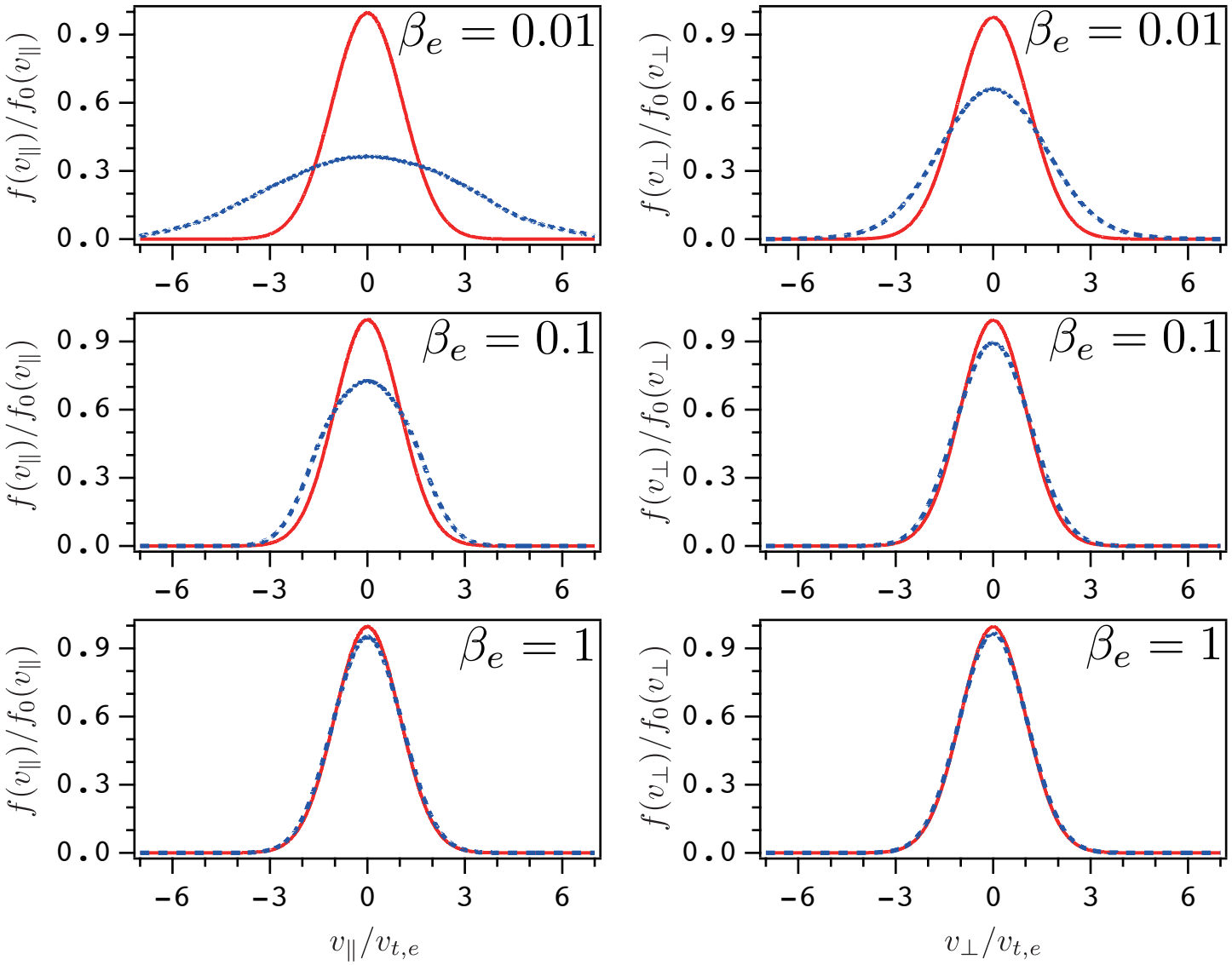
$\beta_e = 0.01$
$\beta_e = 0.01$
$\beta_e = 0.1$
$\beta_e = 0.1$
$\beta_e = 1$
$\beta_e = 1$
$f(v_\parallel)/f_0(v_\parallel)$
$f(v_\perp)/f_0(v_\perp)$
0.0
0.3
0.6
0.9
−6
−3
0
3
6
$v_\parallel/v_{t,e}$
$v_\perp/v_{t,e}$

Figure 5

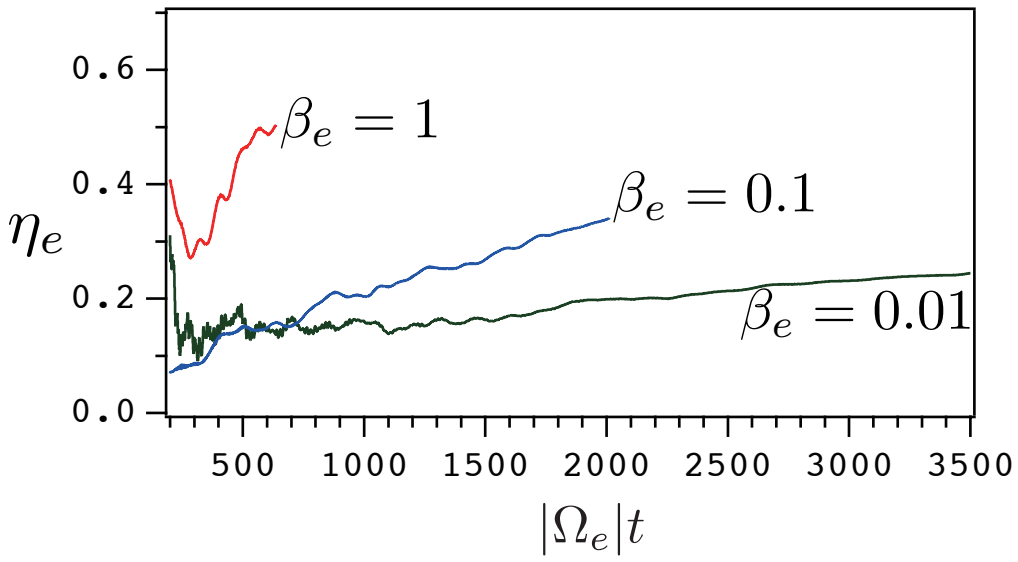
0.6
0.4
0.2
0.0
η_e
$\beta_e = 1$
$\beta_e = 0.1$
$\beta_e = 0.01$
500
1000
1500
2000
2500
3000
3500
$|\Omega_e|t$

Figure 6

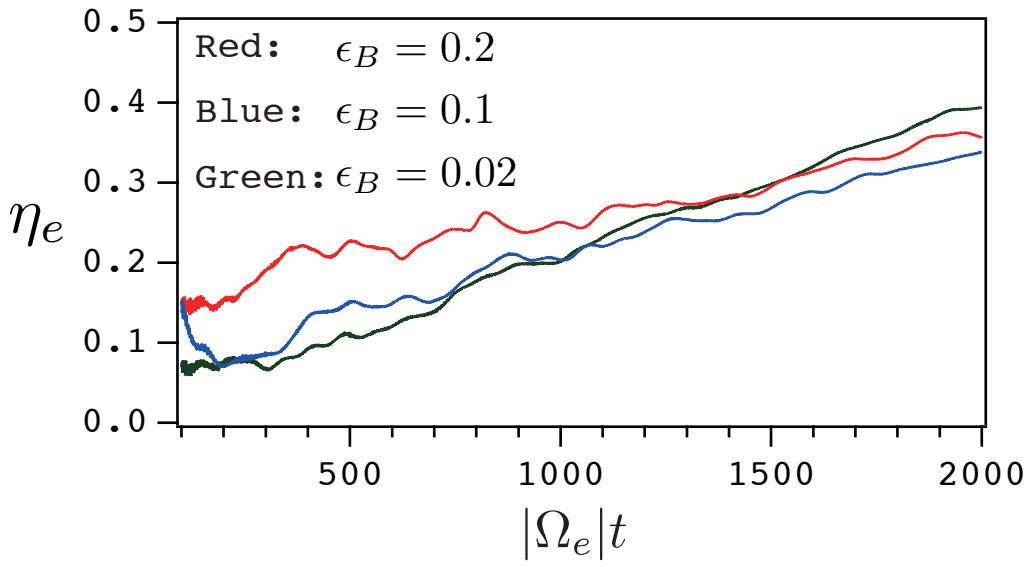
Red: $\epsilon_B = 0.2$
Blue: $\epsilon_B = 0.1$
Green: $\epsilon_B = 0.02$
η_e
0.0
0.1
0.2
0.3
0.4
0.5
500
1000
1500
2000
$|\Omega_e|t$